

RESEARCH ARTICLE

Open Access



Evaluation of the deformation shape of a balloon-type dielectric elastomer actuator prestretched with water pressure

Natsumi Koike[†] and Takeshi Hayakawa^{*†} 

Abstract

In this study, we evaluated the deformation shape of a balloon-type dielectric elastomer actuator (DEA) that has been prestretched with water pressure. We fabricated the DEA with poly(dimethylsiloxane) (PDMS) as the elastomeric material and carbon grease as the electrode. We derived analytical solutions for the deformation of the DEA based on structural mechanical models. Additionally, we compared the deformation shapes obtained by theoretical analysis and experimental results. Our model can partially predict the deformation shape of the DEA with good accuracy. In addition, we discuss the applicable range of the theoretical model and error relative to the experimental results.

Keywords: Soft actuator, Dielectric elastomer actuator (DEA), Structural mechanics

Introduction

Recently, soft actuators have attracted considerable attention because they have the potential to realize biomimetic soft mechanisms [1, 2] or to be used in various new applications, such as human machine cooperation [3] or low-invasive medical robots [4]. Various types of soft actuators have been proposed that are driven by pneumatic [5, 6], electrical [7–9], thermal [10, 11], or optical [12, 13] inputs. Among these types of soft actuators, electrically-driven soft actuators generally have advantages of fast response, small size, low weight, and large deformation. Dielectric elastomer actuators (DEAs) are one type of electrically driven soft actuator. They are driven by high voltage (\approx kV), consist of commercially available soft polymer materials, and are easily fabricated due to their simple structures [14–16]. Since DEAs can be utilized in dry environments, they are potential candidates for practical applications in soft actuators.

Generally, DEAs are composed of thin planar dielectric elastomer materials sandwiched by flexible electrodes on both sides of the elastomer. When we apply a high electric voltage (\approx kV) between the electrodes, the dielectric elastomer becomes thinner but extends in the planar direction because of Maxwell stress between the electrodes. Thus, DEAs are normally actuated in the in-plane direction of the sheet of DEA and are installed in mechanical structures to generate bending motion for practical applications, such as artificial muscles [17–19] or fish robots [20–22]. Here, we note that one important drive condition of a DEA is prestretching of the dielectric elastomer materials. To generate large deformations, dielectric elastomers should be stretched prior to actuation. Most DEAs are stretched in the in-plane direction by using mechanical jigs, which restricts the motions of DEAs in the in-plane direction. Another way to prestretch DEAs is to use air pressure [23] or water pressure [24]. When air or water pressure is applied to a DEA, the shape of the DEA is deformed like a balloon. Thus, the directions of actuation of these types of DEAs are intrinsically out-of-plane and can be applied to loud speakers [25], fluid pumps [26], or tactile presentation devices [27].

*Correspondence: hayaka-t@mech.chuo-u.ac.jp

[†]Natsumi Koike and Takeshi Hay contributed equally to this work
Department of Precision Engineering, Chuo University, Bunkyo, Tokyo, Japan

For detailed studies on prestretched DEAs with air or water pressure, there are several studies on the drive characteristics of balloon-type DEAs [25, 28–30]. These studies have experimentally evaluated static behaviors [30] or dynamic behaviors [25], or have numerically simulated dynamic characteristics of balloon-type DEAs [28, 29]. However, numerical simulations cannot predict the deformation shape of balloon-type DEAs according to various design values, such as diameter, thickness, and pressure [31, 32]. Thus, to design balloon-type DEAs with desired deformation shapes, a predictive analytical model of DEAs with various design parameters must be developed.

In this paper, we perform theoretical and experimental analyses of balloon-type DEA deformations. First, we theoretically and experimentally evaluate static characteristics of DEAs with uniaxial load and compare the results. Second, we derive analytical solutions of the deformations of a balloon-type DEA with water pressure and electric voltage under two assumptions; (i) employing a flexural model of a circular plate and spherical shell in structural mechanics for the analysis, (ii) employing linear constitutive law (Hooke's law) to derive analytical solutions. Then, we compare the analytical results with the experimental results of various sizes of balloon-type DEAs prestretched with water pressure and discuss the validity and applicable range of the model.

Evaluations of DEA with uniaxial load

First, we evaluated DEAs with uniaxial load, which is a commonly used system to evaluate basic characteristics of DEAs. In this study, we used polydimethylsiloxane (PDMS) (Silpot 184, Toray Dow Corning, Tokyo, Japan) for both DEA samples prestretched with a uniaxial load and with water pressure. PDMS is a transparent and heat-curable silicone elastomer and is known to have high formability and a high dielectric coefficient. Furthermore, PDMS is also known to have relatively linear mechanical characteristics over a small deformation region of up to $\approx 50\%$ [33, 34]. This DEA with a uniaxial load was evaluated to confirm the linearity of PDMS as a DEA material. For the theoretical analysis of the deformation shape of the DEA in the next section, we assumed that PDMS has linear characteristics.

Fabrication of DEA

For fabrication of a thin membrane of PDMS, we use a spin coating method commonly used in microfabrication. Liquid PDMS is applied to a polystyrene sheet substrate and spin coated at 1500 rpm for 30 s. Afterwards, liquid PDMS on the substrate were baked at 80 °C for 2 h in a constant-temperature oven. Then, we obtained a PDMS membrane with a thickness of approximately 100 μm .

Finally, the surface of the DEA was coated with carbon grease (MG846-80G, MG Chemicals, Burlington, Canada) as the electrode. We fabricated DEAs at thicknesses of 80, 100, 120 μm by changing the preparation conditions. For each thickness, three samples were fabricated and evaluated.

Experimental system for uniaxial load

A fabricated PDMS membrane was fixed with fixing jigs as shown in Fig. 1a, b. This fixing jigs are made of acrylic plate and sandwiches fabricated PDMS membrane. Furthermore, we put thin PDMS sheets on the fixing jigs to increase friction forces between the jigs and PDMS membrane and firmly fix the PDMS membrane. Additionally,

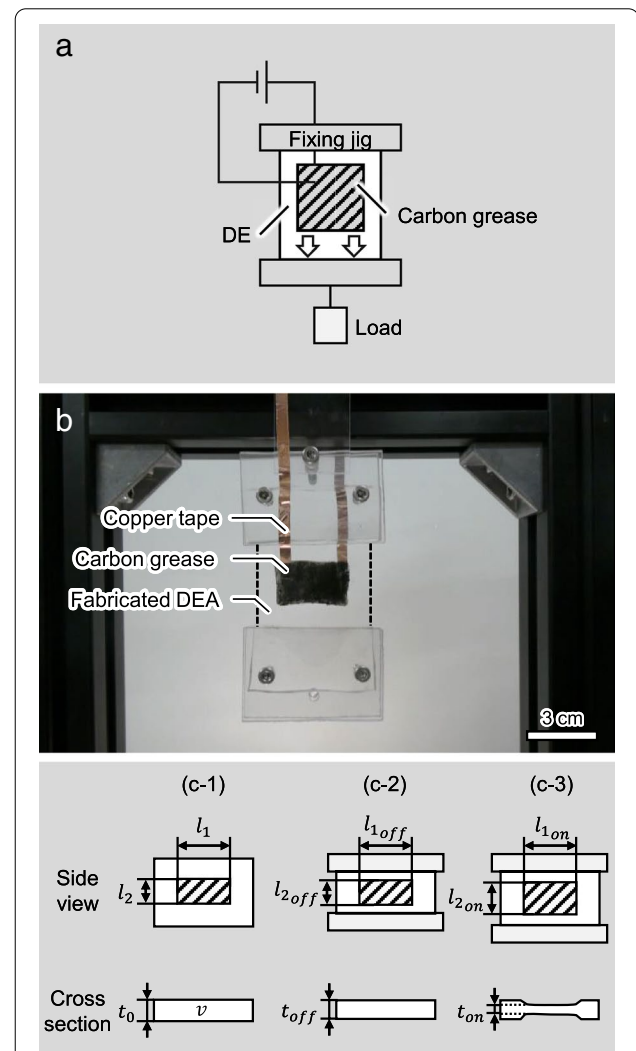


Fig. 1 Experimental system of uniaxial load. **a** Schematic figure of the experimental system, **b** picture of the actual experimental system, **c** schematic figures of deformation of a DEA with uniaxial load

copper tapes were attached to both sides of the PDMS and used for connection to a power supply. This DEA was attached to an aluminum frame and a weight was hanged to the bottom fixing jig to apply uniaxial load. For electric voltage application, we used a function generator (AFG3022C, Tektronix) to generate the input signal. The input signal was connected to a high-voltage amplifier [HOPP-5P(A), Matsusada precision, Shiga, Japan]. In this study, we varied the voltage from 0 to 3.0 kV. Actuator displacement was acquired using digital cameras (DC-TZ90, Panasonic, Osaka, Tokyo) and measured using visual analysis software Image J [35, 36].

Theoretical model of DEA with uniaxial load

Under the assumption that PDMS obeys linear constitutive law (Hooke's law), the relationship between strain of PDMS s_t and voltage V can be written as follows with a simple capacitor model.

$$s_t = \frac{\varepsilon_r \varepsilon_0}{E} \frac{V^2}{t^2}. \quad (1)$$

Here, ε_0 is permittivity of vacuum, E is the Young's modulus of the material, V is an applied electric voltage, and t is a thickness of PDMS. ε_r is relative permittivity, which is 2.72 for Silpot 184. We used this Eq. (1) to evaluate the drive characteristics of the DEA with a uniaxial load.

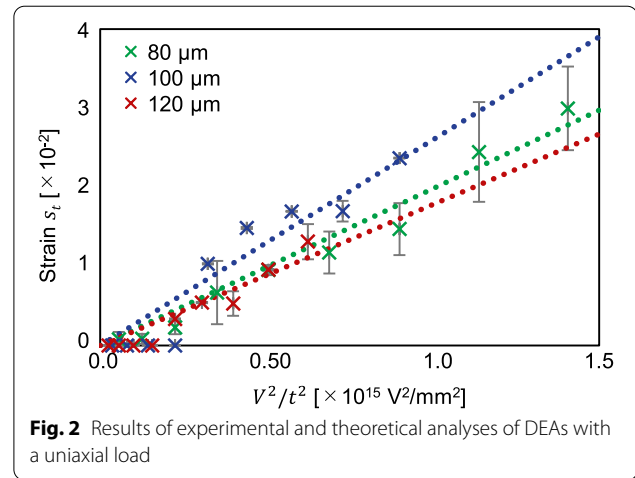
To determine strains s_t of DEA in the experiments, we calculated s_t , as shown in Fig. 1c. The DEA has three phases: first phase without a load (Fig. 1c-1), "off" phase with a load (Fig. 1c-2) and "on" phase with a load and electric voltage (Fig. 1c-3). Here, $l_1, l_2, l_{1off}, l_{2off}, l_{1on}$ and l_{2on} are the electrode widths of every phase, and t_0, t_{off} and t_{on} are the thickness of the elastomer. When we assume that the elastomer is non-compressible, the elastomer volume $v = l_1 l_2 t_0$ is constant for every phase. Then, we can calculate elastomer thickness at the on phase t_{on} by measuring widths and heights of the electrode $l_{1off}, l_{2off}, l_{1on}, l_{2on}$. As a result, we can experimentally calculate thickness strain of the elastomer s_t with the following equations.

$$t_{off} = \frac{v}{l_{1off} l_{2off}}, \quad t_{on} = \frac{v}{l_{1on} l_{2on}} \quad (2)$$

$$s_t = \frac{t_{off} - t_{on}}{t_{off}}$$

Results

Figure 2 shows the experimental results of the actuation of DEA with uniaxial load. To evaluate the strain characteristics of PDMS, we set V^2/t^2 as the horizontal axis and s_t on the vertical axis in Fig. 2. By setting this horizontal axis, this plot should be linear, according to Eq. (1), if the Young's modulus E is constant. In this case, we



can estimate the Young's modulus E from the slope of the line.

In Fig. 2, experimental results of DEA with 80 μm , 100 μm , and 120 μm are shown in green, blue, and red cross points, respectively. Also, we plotted the approximate line linearized by a least-squares method, which is shown as a solid line for each color. From this approximation, the slopes were 1.98, 2.60, and 1.78×10^{-17} for DEA with thicknesses of 80 μm , 100 μm , and 120 μm , respectively. From these results, the Young's modulus of the fabricated PDMS varied from 0.825 to 1.21 MPa. These values are thought to vary due to the curing conditions or fabrication error of the thickness. For theoretical analysis in the next section, we use 0.80 MPa as the value of the Young's modulus of PDMS.

Evaluations of DEA only with water pressure

Second, we evaluated the deformation of DEA with water pressure, which is the main target of this study. The systems were previously reported by Godaba et al. [37] to realize large deformation in the out-of-plane direction of a DEA. In this study, we fabricated balloon shaped DEAs made of PDMS and evaluated the deformation shape.

Fabrication of DEA

For the fabrication of thin membranes of PDMS, we used a spin coating method similar to the DEA with uniaxial load in the previous section. In this case, we fabricated DEAs with thicknesses of 100 μm , and three samples were fabricated and evaluated at each condition.

Experimental system for water pressure

For prestretching with water pressure, we used an experimental system to apply water pressure by connecting a water reservoir and a circular pipe with a hose, as shown in Fig. 3a, b. The fabricated PDMS

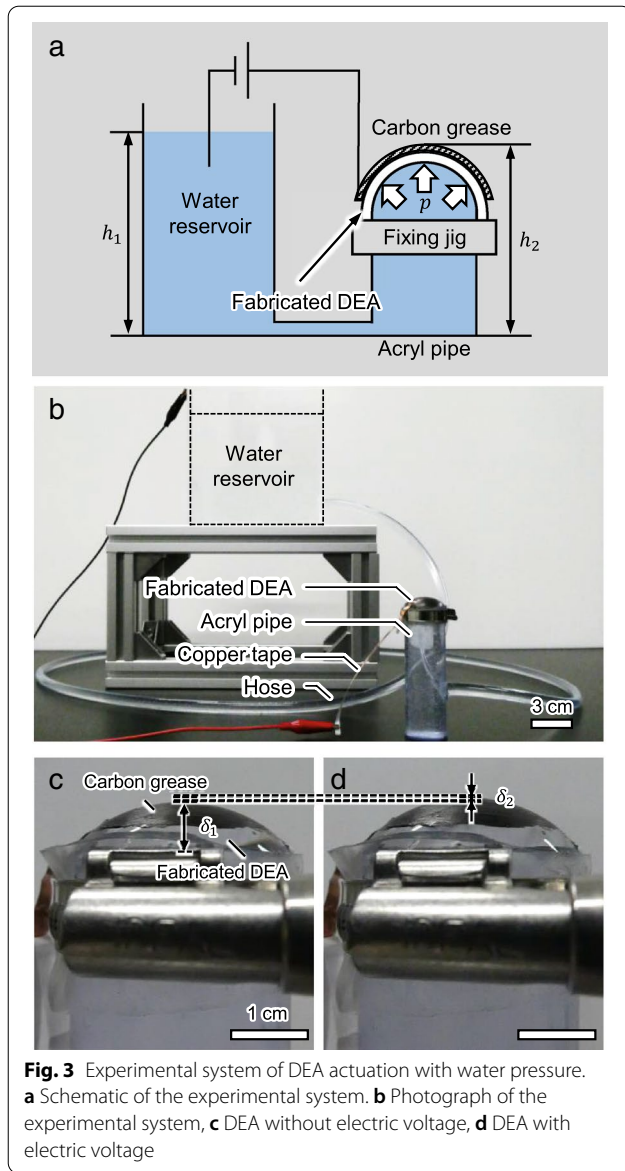


Fig. 3 Experimental system of DEA actuation with water pressure. **a** Schematic of the experimental system, **b** Photograph of the experimental system, **c** DEA without electric voltage, **d** DEA with electric voltage

membrane was affixed to an acrylic pipe. After that, the surface of the DEA was coated with carbon grease. In this study, we used acrylic pipes with diameters of 18.0, 24.0, and 32.0 mm.

In using this system, water pressure for prestretching can be changed by the height of water in the reservoir. Water pressure p applied to DEA is determined as follows.

$$p = \rho g(h_1 - h_2) \quad (3)$$

Here, ρ is density of water, g is acceleration of gravity, h_1 and h_2 are heights of water in the reservoir and the pipe, as shown in Fig. 3a. Additionally, water was also used as an electrode to apply electric voltage to the DEA. We

connected the grand electrode of the high voltage amplifier to the water reservoir.

Analytical solution of the deformation of DEAs only with water pressure

To theoretically analyze deformations of DEAs with water pressure, we employed following two assumptions; (i) PDMS membrane is analyzed by using a flexural model of a circular plate. (ii) PDMS membrane has linear constitutive law (Hooke's law). We assume PDMS has linear elastic properties in our model because PDMS is known to have linear characteristics until $\approx 50\%$ deformation [33, 34], as we confirmed in the previous section. To analyze deformations of DEA, we consider that there are three phases of DEA actuation in our system, as shown in Fig. 4a. First, before applying water pressure to the membrane, the membrane had a circular disk shape, as shown in Fig. 4a, b. Second, when we applied water pressure to the membrane, the membrane expanded as a curved surface, and the displacement was determined as $\delta_1(r)$, as shown in Fig. 4a, c. Here, r is the radial coordinate of the circular plate. Third, when we applied electric voltage to the membrane, it expanded further according to the electrostatic voltage, and we determined this displacement as $\delta_2(r)$, as shown in Fig. 4a, d. Therefore, total displacement of the DEA $\delta(r)$ is written as follows and it is a function of r .

$$\delta(r) = \delta_1(r) + \delta_2(r) \quad (4)$$

We analyzed the deformation of the DEA by using two models: (i) circumferentially supported disk model with distributed load for water pressure: $\delta_1(r)$ (Fig. 4c) and (ii) the curvature shell model with distributed load for an electric voltage: $\delta_2(r)$ (Fig. 4d) [33].

We assume that the membrane is a disk supported at its circumference, and the distributed load is applied to the disk to express prestretching with water pressure, as shown in Fig. 4c. Normally, deflection $\delta_1(r)$ can be calculated by solving infinitesimal deformation models of the disk. However, when the out-of-plane deformation of the disk is larger than the thickness of the disk, the infinitesimal deformation model is not valid and this large deflection can be solved by using the energy method [38]. Thus, we employed the energy method for the analysis of our system. Considering conservation of energy, deflection energy of the disk U is a sum of bending energy U_1 and expanding energy U_2 and these can be written as follows.

$$U_1 = \frac{1}{2} \int_0^{2\pi} \int_0^a \left(M_r \frac{1}{R_1} + M_\theta \frac{1}{R_2} r \right) d\theta dr \quad (5)$$

$$U_2 = \frac{1}{2} \int_0^{2\pi} \int_0^a (N_r \varepsilon_r + N_\theta \varepsilon_\theta r) d\theta dr \quad (6)$$

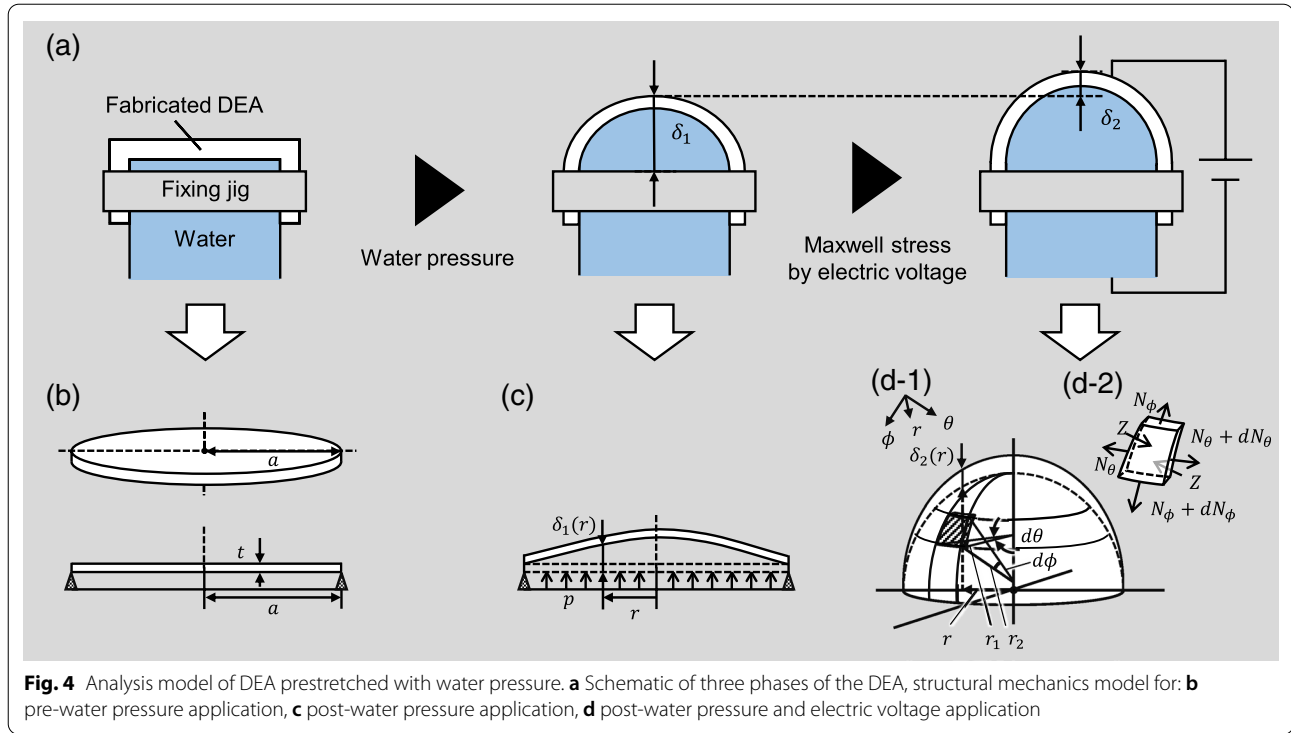


Fig. 4 Analysis model of DEA prestretched with water pressure. **a** Schematic of three phases of the DEA, structural mechanics model for: **b** pre-water pressure application, **c** post-water pressure application, **d** post-water pressure and electric voltage application

Here, M_r and M_θ are bending moments, R_1 and R_2 are curvature radii in r and θ directions, respectively. Also, N_r , N_θ are stresses and ε_r , ε_θ are strains of the middle surface in the r and θ directions, respectively. By using a relationship of bending moments M_r , M_θ , curvature radii R_1 , R_2 , and bending rigidity $D = Et^3/12(1 - \nu^2)$, U_1 can be written as follows.

$$U_1 = -\frac{D}{2} \int_0^{2\pi} \int_0^a \left[\left(\frac{1}{R_1} + \frac{\nu}{R_2} \right) \frac{1}{R_1} + \left(\frac{1}{R_1} + \frac{\nu}{R_2} \right) \frac{1}{R_1} \right] r d\theta dr \quad (7)$$

Here, ν is the Poisson's ratio of the material. Furthermore, curvatures R_1 and R_2 can be rewritten by derivatives of deflection δ_1 by using geometric relationships as follows.

$$U_1 = \pi D \int_0^a \left[\left(\frac{d^2 \delta_1}{dr^2} \right)^2 + \frac{1}{r^2} \left(\frac{d \delta_1}{dr} \right)^2 + 2\nu \frac{1}{r} \frac{d \delta_1}{dr} \frac{d^2 \delta_1}{dr^2} \right] r dr. \quad (8)$$

Next, U_2 can be written as follows by using a relationship between stress N_r , N_θ , and strain ε_r , ε_θ .

$$U_2 = \frac{\pi t E}{(1 - \nu^2)} \int_0^a \left[(\varepsilon_r + \varepsilon_\theta)^2 - 2(1 - \nu) \varepsilon_r \varepsilon_\theta \right] r dr \quad (9)$$

When we set a displacement in the radial direction as $u(r)$, ε_θ and ε_r can be written by using $u(r)$ as follows.

$$\varepsilon_\theta = \frac{2\pi(r + u) - 2\pi r}{2\pi r} = \frac{u}{r}, \quad (10)$$

$$\varepsilon_r = \frac{du}{dr} + \frac{1}{2} \left(\frac{d\omega}{dr} \right)^2 \quad (11)$$

Thus, U_2 can be rewritten as the following equation by using Eqs. (9), (10) and (11), as follows.

$$U_2 = \frac{\pi E t}{1 - \nu^2} \int_0^a \left[\left(\frac{du}{dr} \right)^2 + \frac{1}{4} \left(\frac{d \delta_1(r)}{dr} \right)^4 + \frac{du}{dr} \left(\frac{d \delta_1(r)}{dr} \right)^2 + \frac{u^2}{r^2} + 2\nu \frac{u}{r} \left\{ \frac{du}{dr} + \frac{1}{2} \left(\frac{d \delta_1(r)}{dr} \right)^2 \right\} \right] r dr. \quad (12)$$

Here, we assume that the deflection of the disk $\delta_1(r)$ can be written as follows, which is written in analogously to the infinitesimal deformation model.

$$\delta_1(r) = \delta_1(0) \left(1 - \frac{r^2}{a^2} \right)^2 \left(1 - \frac{5 + \nu}{1 + \nu} \frac{r^2}{a^2} \right) \quad (13)$$

In our model, a circumferential supported disk with distributed load should not deform at the center and

circumference in the radial direction. Thus, radial displacement $u(r)$ can be written under these boundary conditions as follows.

$$\begin{aligned} u &= r(a-r)(c_0 + c_1r + c_2r^2 + \dots) \\ &= c_0ar + (ac_1 - c_0)r^2 + \dots \end{aligned} \quad (14)$$

Here, c_0, c_1, c_2, \dots are undetermined constants, and we used the second-order term of this equation in this study. c_0 and c_1 can be determined as the strain energy U , which become the minimum turning points as follows.

$$\frac{dU}{dc_0} = 0, \quad \frac{dU}{dc_1} = 0. \quad (15)$$

Then, we acquire following values for c_0 and c_1 by calculating integral of Eq. (12).

$$c_0 = 0.799 \frac{\delta_1(0)^2}{a^3}, \quad c_1 = -0.148 \frac{\delta_1(0)^2}{a^4} \quad (16)$$

Here, we used the value of $\nu = 0.5$. By using these values of c_0 and c_1 , we can calculate U_1 and U_2 as follows.

$$U_1 = 0.441\pi \frac{Et^3}{a^2} \delta_1(0)^2 \quad (17)$$

$$U_2 = 0.402\pi \frac{Et}{a^2} \delta_1(0)^4 \quad (18)$$

Virtual work W by external force p can be calculated as:

$$W = \int_0^{2\pi} \int_0^a p \delta_1(r) r d\theta dr = \frac{5}{11} \pi a^2 p \delta_1(0). \quad (19)$$

By using Eqs. (17)–(19), the minimum deflection energy U_{min} can be derived by the following equation.

$$\frac{d(U_{min} - W)}{d\delta_1(0)} = 0 \quad (20)$$

From this condition, we acquire the following equation.

$$0.882 \frac{E}{a^2} t^3 \delta_1(0) + 1.61 \frac{E}{a^2} t \delta_1(0)^3 = \frac{5}{11} a^2 p \quad (21)$$

In the case of the deflection $\delta_1(0)$ is much larger than the thickness of the disk t , the first term is negligible. This approximation is equivalent to ignore the bending energy U_1 . Then, we acquire the maximum deflection $\delta_1(0)$ by solving Eq. (21) and it can be written as follows.

$$\delta_1(0) = 0.657a \left(\frac{pa}{Et} \right)^{\frac{1}{3}}. \quad (22)$$

From Eqs. (13) and (22), $\delta_1(r)$ can be written as follows.

$$\delta_1(r) = 0.657a \left(\frac{pa}{Et} \right)^{\frac{1}{3}} \left(1 - \frac{r^2}{a^2} \right)^2 \left(1 - \frac{11}{3} \frac{r^2}{a^2} \right) \quad (23)$$

Results

Then, we experimentally and theoretically evaluated the deformation of DEA with prestretching by water pressure. Figure 5a, b are typical examples of $\delta_1(r)$ acquired by experimental and theoretical calculations. These results were acquired with conditions of $p = 1.37$ (kPa), $a = 16.0$ (mm), $\nu = 0.5$, and $E = 0.80$ (MPa). The experimental picture from the side and the perspective view of theoretical results seem to be in a good agreement with these shapes. Additionally, the maximum displacements at the top of the DEA $\delta_1(0)$ are 7.84 mm in experiments and 7.71 mm in analysis, and these values agree well.

Next, we compared the experimental results and theoretical results with various diameters of acrylic pipes and water pressures. Figure 5c, d show the cross-sectional view of the $\delta_1(r)$ at the center of the DEA. In the results in Fig. 5c, water pressures of 1.37 kPa were applied to DEA with diameters of acrylic pipe $a = 9, 13, 16$ mm. Additionally, In Fig. 5d, water pressures of 1.17 kPa, 1.27 kPa, and 1.37 kPa are applied to DEA with an acrylic pipe radius of 16 mm. These results, especially the results of $a = 9$ and 13 mm in Fig. 5c, theoretical and experimental are quantitatively in good agreement.

Evaluation of DEA with water pressure and electric voltage

Analytical solution of deformation of DEA with water pressure and electric voltage

To evaluate the deflection δ_2 of the membrane with water pressure and electric voltage, we again employed following two assumptions similar to the previous section; (i) PDMS membrane is analyzed by using a flexural model of a spherical shell. (ii) PDMS membrane has linear constitutive law (Hooke's law). We treat the electrostatic force generated by applying electric voltage as a distributed load on the membrane. First, we assumed the equilibrium of the force of infinitesimal area, as shown in Fig. 4d-2. The area is subjected to forces in the circumferential N_θ and meridional directions N_ϕ , and electrostatic force is applied in the normal direction of the area Z . These forces are written as follows.

$$N_\theta = \frac{r_2}{2} Z, \quad N_\phi = -\frac{3}{2} r_1 Z \quad (24)$$

Here, r_1, r_2 are curvature radii in each direction. These forces cause strain $\varepsilon_\theta, \varepsilon_\phi$ in each direction and these are written as follows.

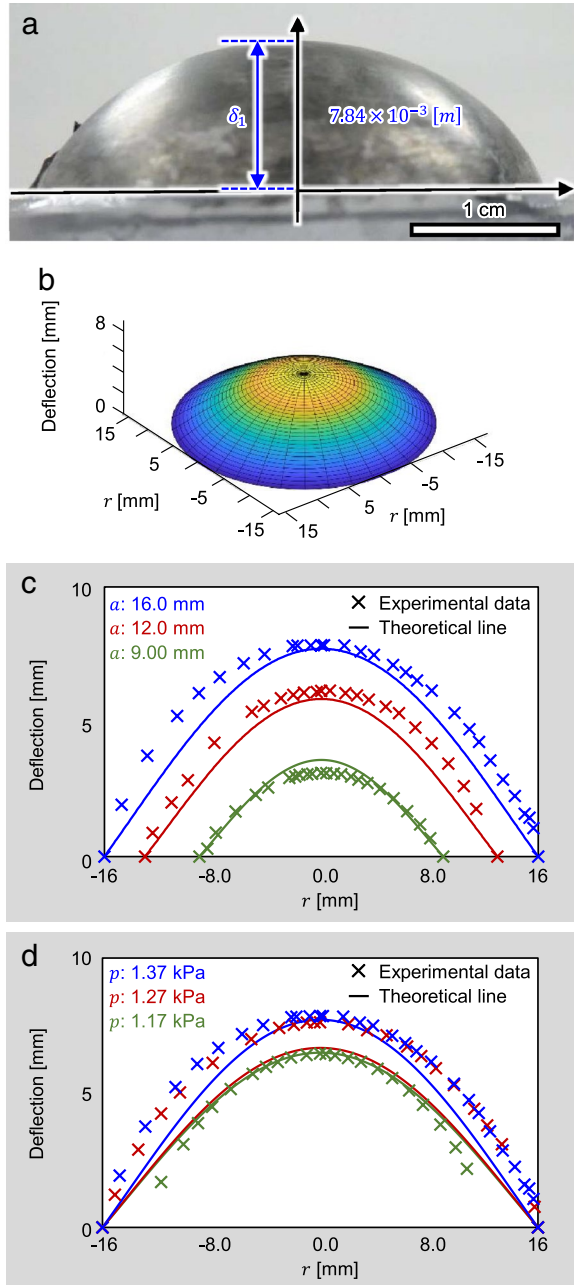


Fig. 5 Evaluation of DEA with water pressure. **a** Experimental picture of DEA with a water pressure of 1.37 kPa. **b** 3D plot of the analytical solution of Eq. 23. **c** Comparison of theoretical and experimental data with changing diameter a . **d** Comparison of theoretical and experimental data with changing pressure p

$$\varepsilon_\theta = \frac{\nu}{r_2} \cot \phi - \frac{\delta_2(\phi)}{r_2}, \quad \varepsilon_\phi = \frac{1}{r_1} \frac{d\nu}{d\phi} - \frac{\delta_2(\phi)}{r_2} \quad (25)$$

where ν is displacement in the tangential direction of the meridian and δ_2 is the displacement of the normal

direction of the middle surface. By using Hooke's law, these equations can be written as follows.

$$\varepsilon_\theta = \frac{1}{Et} (N_\phi - \nu_\theta), \quad \varepsilon_\phi = \frac{1}{Et} (N_\theta - \nu N_\phi) \quad (26)$$

Here, t is the thickness of the membrane. Then, deflection of the shell $\delta_2(\phi)$ is derived by Eqs. (24), (25) and (26), as follows.

$$\delta_2(\phi) = \frac{r^2 \cos^2 \phi}{1 - r^2 \cos^2 \phi} \frac{1}{Et} \times \left[r_1 (N_\phi - \nu N_\theta) - \frac{r_2}{\cos^2 \phi (N_\theta - \nu N_\phi)} \right] \quad (27)$$

Finally, we acquired the equation of deflection of the DEA $\delta(r)$ as a function of water pressure p and electrostatic force Z is written as follows.

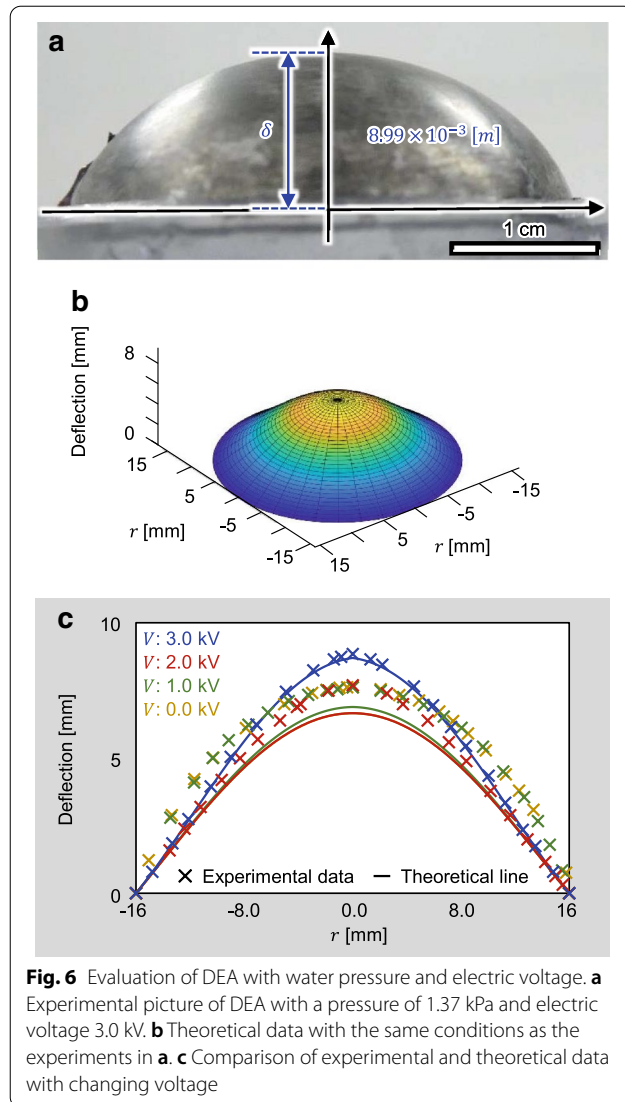
$$\begin{aligned} \delta(r) &= \delta_{1(r)} + \delta_{2(r)} = \delta_{1(r)} + \delta_2(\phi) \cos \phi \\ &= 0.657a \left(\frac{pa}{Et} \right)^{\frac{1}{3}} \left(1 - \frac{r^2}{a^2} \right)^2 \left(1 - \frac{11}{3} \frac{r^2}{a^2} \right) \\ &\quad + \frac{r^2 \cos^3 \phi}{1 - r^2 \cos^2 \phi} \frac{1}{Et} \\ &\quad \times \left[\frac{r_1}{2} (r_2 + 1.5r_1) Z - \frac{2r_2}{\cos^2 \phi (r_2 + 1.5)Z} \right], \\ Z &= \varepsilon_r \varepsilon_0 \frac{V^2}{t^2} \end{aligned} \quad (28)$$

Here, ε_r and ε_0 are dielectric permittivity of PDMS and vacuum, respectively.

Results

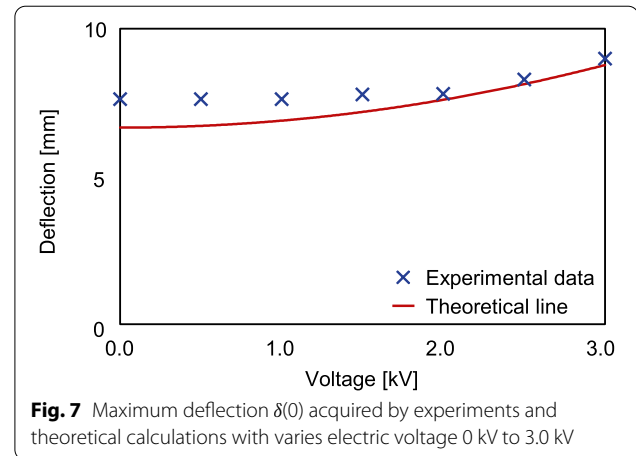
Then, we also experimentally and theoretically evaluate the deformation of DEA with water pressure and electric voltage. Figure 6a, b are typical examples of $\delta(r) = \delta_1(r) + \delta_2(r)$ that are acquired by experiments and theoretical calculations, respectively. These results were acquired with conditions of $p = 1.37$ (kPa), $a = 16$ (mm), $\nu = 0.50$, $E = 0.80$ (MPa) and $V = 3.0$ (kV). The experimental picture and theoretical results seem to be in good agreement with these shapes. Additionally, the maximum displacement at the top of the DEA $\delta(0)$ was 8.99 mm in the experiments and 8.84 mm in analysis. The values of deformation $\delta(0)$ acquired with experiments and theoretical calculations are slightly different.

Next, we compared experimental results and theoretical results with various electric voltages. Figure 6c shows the cross-sectional view of the $\delta(r)$ at the center of the DEA. In the results in Fig. 6c, water pressure $p = 1.37$ (kPa), and electric voltage V is varied as 1.0, 2.0, and 3.0 kV. These experimental and theoretical



results are qualitatively in agreement but the values are a little different. This difference is thought to be caused because of assumptions of our model. We assume that the actuator has shapes of a part of spherical shell and uniform thickness, as shown in Fig. 4d. However, actual actuators might have different shapes and non-uniform thicknesses.

We also evaluated the maximum deflections at the center of the DEA $\delta(0)$, by applying electric voltage from 0 to 3.0 kV, as shown in Fig. 7. From Fig. 7, the maximum differences of theoretical values from experimental values are +0.40/−0.15 mm and these values are +5.15/−1.64% of $\delta(0)$. Thus, our model is suitable for predicting the values of the maximum deformation $\delta(0)$ of the DEA in our system.



Discussion

Here, we note the actual values of strains of PDMS and discuss the applicable range of our model. Basically, we analyzed the deformation of DEA by assuming that PDMS has linear mechanical characteristics. References [33, 34] shows that PDMS has almost linear mechanical characteristics up to 50% strain. Thus, we derived the deformation of DEA with water pressure and electric voltage with a constant Young's modulus. By using this model, we acquired quantitatively good results in $a = 9$ and 13 mm conditions in Fig. 5c. However, the results in $a = 16$ mm and the theoretical results are a little different from experimental values. It is thought to be because of the large deformation of the PDMS.

Thickness strains of PDMS in conditions of $a = 9$ and 13 mm in Fig. 5c are 53.7% and 56.4%, respectively. These values exceed the value 50%. However, the results of deformation in these conditions are quantitatively in good agreement with experiments. On the other hand, thickness strain of PDMS in condition of $a = 16$ mm in Fig. 5c is 57.1% and theoretical results in this condition are quantitatively in not good agreement with experiments. Thus, the thickness strain $\approx 55\%$ is thought to be a border of the applicable range of our model assuming linear mechanical characteristics of PDMS. Under this value of thickness strain, our model is thought to be applicable to quantitatively predict deformation shapes of the balloon-type DEA made of PDMS. These limitation can be resolved by introducing nonlinear characteristics of the material as studied in Ref. [39] However, for larger strain as shown in Figs. 6 and 7, the deformation shapes of the theoretical results are qualitatively in agreement with the experimental value and maximum deformation $\delta(0)$ can be acquired within the error of +5.15/−1.64%.

Conclusions

In this study, we analyzed deformation shape of balloon-type DEA prestretched with water pressure. We derived the analytical solution of the deformation shape based on structural mechanics. We evaluated deformation of the balloon-type DEA with theoretical calculations and experiments and compared them. Theoretical results of our model are quantitatively in good agreement with experimental results up to $\approx 55\%$ of thickness strains. Thus, the model can be used to design the balloon-type DEA with desired deformation.

Acknowledgements

This research is supported by Chuo University Personal Research Grant, Chuo University Grant for Special Research, and Grant of the Hattori Hokokai Foundation.

Authors' contributions

NK and TH conceiving and designing the study, collecting data, performing the analysis and interpretation of data, drafting the manuscript, and critically revising the manuscript. Both authors read and approved the final manuscript

Funding

This research is supported by Chuo University Personal Research Grant, Chuo University Grant for Special Research, and Grant of the Hattori Hokokai Foundation.

Availability of data and materials

Not applicable.

Competing interests

The authors declare that they have no competing interests.

Received: 26 September 2020 Accepted: 8 January 2021

Published online: 18 January 2021

References

1. Wehner M, Truby RL, Fitzgerald DJ, Mosadegh B, Whitesides GM, Lewis JA, Wood RJ (2016) An integrated design and fabrication strategy for entirely soft, autonomous robots. *Nature* 536(7617):451–455
2. Coyle S, Majidi C, LeDuc P, Hsia KJ (2018) Bio-inspired soft robotics: material selection, actuation, and design. *Extreme Mech Lett* 22:51–59
3. Vanderborght B, Van Ham R, Verrelst B, Van Damme M, Lefeber D (2008) Overview of the lily project: dynamic stabilization of a biped powered by pneumatic artificial muscles. *Adv Robot* 22(10):1027–1051
4. Gerboni G, Diodato A, Ciuti G, Cianchetti M, Menciassi A (2017) Feedback control of soft robot actuators via commercial flex bend sensors. *IEEE/ASME Trans Mechatron* 22(4):1881–1888
5. Caldwell DG, Medrano-Cerda GA, Goodwin M (1995) Control of pneumatic muscle actuators. *IEEE Control Syst Mag* 15(1):40–48
6. Li C, Xie Y, Li G, Yang X, Jin Y, Li T (2015) Electromechanical behavior of fiber-reinforced dielectric elastomer membrane. *Int J Smart Nano Mater* 6(2):124–134
7. Li Y, Hashimoto M (2015) Pvc gel based artificial muscles: characterizations and actuation modular constructions. *Sens Actuators A Phys* 233:246–258
8. Kim B, Lee MG, Lee YP, Kim Y, Lee G (2006) An earthworm-like micro robot using shape memory alloy actuator. *Sens Actuators A Phys* 125(2):429–437
9. Lee S-G, Park H-C, Pandita SD, Yoo Y (2006) Performance improvement of ipmc (ionic polymer metal composites) for a flapping actuator. *Int J Control Autom Syst* 4(6):748–755
10. Ware TH, McConney ME, Wie JJ, Tondiglia VP, White TJ (2015) Voxellated liquid crystal elastomers. *Science* 347(6225):982–984
11. Yang Y, Pei Z, Li Z, Wei Y, Ji Y (2016) Making and remaking dynamic 3d structures by shining light on flat liquid crystalline vitrimer films without a mold. *J Am Chem Soc* 138(7):2118–2121
12. Iamsaard S, Alshoff SJ, Matt B, Kudernac T, Cornelissen JJ, Fletcher SP, Katsonis N (2014) Conversion of light into macroscopic helical motion. *Nat Chem* 6(3):229–235
13. Palagi S, Mark AG, Reigh SY, Melde K, Qiu T, Zeng H, Parmeggiani C, Martella D, Sanchez-Castillo A, Kapernaum N (2016) Structured light enables biomimetic swimming and versatile locomotion of photoresponsive soft microrobots. *Nat Mater* 15(6):647–653
14. Pelrine R, Kornbluh R, Joseph J, Heydt R, Pei Q, Chiba S (2000) High-field deformation of elastomeric dielectrics for actuators. *Mater Sci Eng C* 11(2):89–100
15. Chiang Foo C, Cai S, Jin Adrian Koh S, Bauer S, Suo Z (2012) Model of dissipative dielectric elastomers. *J Appl Phys* 111(3):034102
16. Xu L, Chen H-Q, Zou J, Dong W-T, Gu G-Y, Zhu L-M, Zhu X-Y (2017) Bio-inspired annelid robot: a dielectric elastomer actuated soft robot. *Bioinspir Biomim* 12(2):025003
17. Cao J, Liang W, Zhu J, Ren Q (2018) Control of a muscle-like soft actuator via a bioinspired approach. *Bioinspir Biomim* 13(6):066005
18. Acome E, Mitchell S, Morrissey T, Emmett M, Benjamin C, King M, Radakovitz M, Keplinger C (2018) Hydraulically amplified self-healing electrostatic actuators with muscle-like performance. *Science* 359(6371):61–65
19. Gupta U, Wang Y, Ren H, Zhu J (2018) Dynamic modeling and feedforward control of jaw movements driven by viscoelastic artificial muscles. *IEEE/ASME Trans Mechatron* 24(1):25–35
20. Li T, Li G, Liang Y, Cheng T, Dai J, Yang X, Liu B, Zeng Z, Huang Z, Luo Y (2017) Fast-moving soft electronic fish. *Sci Adv* 3(4):1602045
21. Li T, Zou Z, Mao G, Yang X, Liang Y, Li C, Qu S, Suo Z, Yang W (2019) Agile and resilient insect-scale robot. *Soft Robot* 6(1):133–141
22. Cao C, Burgess S, Conn AT (2019) Toward a dielectric elastomer resonator driven flapping wing micro air vehicle. *Front Robot AI* 5:137
23. Mao G, Huang X, Diab M, Li T, Qu S, Yang W (2015) Nucleation and propagation of voltage-driven wrinkles in an inflated dielectric elastomer balloon. *Soft Matter* 11(33):6569–6575
24. Li Z, Zhu J, Foo CC, Yap CH (2017) A robust dual-membrane dielectric elastomer actuator for large volume fluid pumping via snap-through. *Appl Phys Lett* 111(21):212901
25. Hosoya N, Masuda H, Maeda S (2019) Balloon dielectric elastomer actuator speaker. *Appl Acoust* 148:238–245
26. Ho S, Banerjee H, Foo YY, Godaba H, Aye WMM, Zhu J, Yap CH (2017) Experimental characterization of a dielectric elastomer fluid pump and optimizing performance via composite materials. *J Intell Mater Syst Struct* 28(20):3054–3065
27. Mun S, Yun S, Nam S, Park SK, Park BJ, Lim JM, Kyung K-U (2018) Electro-active polymer based soft tactile interface for wearable devices. *IEEE Trans Haptics* 11(1):15–21
28. Zhu J, Cai S, Suo Z (2010) Nonlinear oscillation of a dielectric elastomer balloon. *Polym Int* 59(3):378–383
29. Zhu J, Cai S, Suo Z (2010) Resonant behavior of a membrane of a dielectric elastomer. *Int J Solids Struct* 47(24):3254–3262
30. Keplinger C, Li T, Baumgartner R, Suo Z, Bauer S (2012) Harnessing snap-through instability in soft dielectrics to achieve giant voltage-triggered deformation. *Soft Matter* 8(2):285–288
31. Ahmadi S, Gooyers M, Soleimani M, Menon C (2013) Fabrication and electromechanical examination of a spherical dielectric elastomer actuator. *Smart Mater Struct* 22(11):115004
32. Pourazadi S, Ahmadi S, Menon C (2015) On the design of a dea-based device to potentially assist lower leg disorders: an analytical and fem investigation accounting for nonlinearities of the leg and device deformations. *Biomed Eng Online* 14(1):1–18
33. Molberg M, Leterrier Y, Plummer CJ, Walder C, Löwe C, Opris DM, Nüesch FA, Bauer S, Manson J-AE (2009) Frequency dependent dielectric and mechanical behavior of elastomers for actuator applications. *J Appl Phys* 106(5):054112
34. Kim HT, Jeong OC (2012) Measurement of nonlinear mechanical properties of surfactant-added poly (dimethylsiloxane). *Jpn J Appl Phys* 51(6S):06–07
35. Schneider CA, Rasband WS, Eliceiri KW (2012) NIH image to imagej: 25 years of image analysis. *Nat Methods* 9(7):671–675

36. Abràmoff MD, Magalhães PJ, Ram SJ (2004) Image processing with imagej. *Biophoton Int* 11(7):36–42
37. Godaba H, Foo CC, Zhang ZQ, Khoo BC, Zhu J (2014) Giant voltage-induced deformation of a dielectric elastomer under a constant pressure. *Appl Phys Lett* 105(11):112901
38. Timoshenko SP, Woinowsky-Krieger S (1959) *Theory of plates and shells*. McGraw-hill, NewYork
39. Mao G, Huang X, Liu J, Li T, Qu S, Yang W (2015) Dielectric elastomer peristaltic pump module with finite deformation. *Smart Mater Struct* 24(7):075026

Publisher's Note

Springer Nature remains neutral with regard to jurisdictional claims in published maps and institutional affiliations.

Submit your manuscript to a SpringerOpen[®] journal and benefit from:

- Convenient online submission
- Rigorous peer review
- Open access: articles freely available online
- High visibility within the field
- Retaining the copyright to your article

Submit your next manuscript at ► [springeropen.com](https://www.springeropen.com)
